Vol. 80: 77–92, 2017
https://doi.org/10.3354/ame01842

AQUATIC MICROBIAL ECOLOGY
Aquat Microb Ecol

Published online August 21

Monitoring natural phytoplankton communities: a comparison between traditional methods and pulse-shape recording flow cytometry

L. Haraguchi[1,*], H. H. Jakobsen[1], N. Lundholm[2], J. Carstensen[1]

[1]Department of Bioscience, Aarhus University, 4000 Roskilde, Denmark
[2]Natural History Museum of Denmark, University of Copenhagen, 1307 Copenhagen K, Denmark

ABSTRACT: The phytoplankton community can vary within hours (physiology) to years (climatic and anthropogenic responses), and monitoring at different timescales is relevant for understanding community functioning and assessing changes. However, standard techniques used in monitoring programmes are time-consuming and/or expensive, limiting sampling frequency. The use of faster methods, such as flow cytometry, has become more frequent in phytoplankton studies, although comparisons between this technique and traditional ones are still scarce. This study aimed to assess if natural phytoplankton communities analysed with pulse-shape recording flow cytometry (PFCM) and classical techniques (chl *a* extracts and microscopy) provide comparable results. Monthly samples (March to September 2015) from 4 stations in Roskilde Fjord (Denmark) were analysed with PFCM and classical techniques. Results showed a highly significant correlation between total red fluorescence and chl *a*, and comparable cell counts from PFCM and microscopy for cell sizes >5 µm, but not for sizes <5 µm. We propose an empirical algorithm to obtain cell volumes from the integrated forward scatter signal from PFCM, making it possible to estimate carbon biomass with PFCM, applying the same conversion factors as for microscopy. Biomasses obtained with PFCM, estimated from live cells, were higher than microscopy for natural samples. We conclude that PFCM results are comparable to classical techniques, yet the data from PFCM had poor taxonomic resolution without support of other techniques. With the faster analysis capacity of PFCM, post-processing of data and analysis of high-resolution time series may be made easier.

KEY WORDS: Phytoplankton · Pulse-shape recording flow cytometry · Microscopy · Monitoring · Biomass · Timescale

INTRODUCTION

Phytoplankton constitute the base of most marine food-webs supplying energy to higher trophic levels. The composition of the phytoplankton community therefore plays a key role in trophic interactions. Processes stimulating phytoplankton growth and loss are generally well understood. In contrast, our understanding of mechanisms structuring complex natural phytoplankton communities remains poor. This applies in particular to coastal ecosystems, where the structure of the phytoplankton community may change rapidly. One reason for the poor understanding of processes driving phytoplankton communities is the lack of high-resolution time series describing changes at timescales shorter than phytoplankton generation times (typically days; Harris 1980, Reynolds 2006).

Today, phytoplankton monitoring is used to assess water quality status (Marshall et al. 2006, Salmaso et al. 2006, Boyer et al. 2009), ecosystem services (McGrady-Steed et al. 1997, Falkowski et al. 1998), and the occurrence of toxic species with the aim of mitigating potential effects of harmful algal blooms (Hoagland et al. 2002, Hinder et al. 2011, Campbell

*Corresponding author: luh@bios.au.dk

et al. 2013). However, the sampling frequency of phytoplankton monitoring data for such purposes is generally low, due to the relatively high monitoring costs. The mismatch between sampling frequency and the temporal dynamics of the phytoplankton processes to be monitored can result in considerable uncertainty (Rutten et al. 2005, Winder & Cloern 2010). Important phenomena such as phytoplankton blooms could be overlooked even with weekly sampling (Campbell et al. 2010), which for most monitoring programmes is considered intensive sampling. Hence, there is a need for fast monitoring methods that can deliver reliable information on the phytoplankton community with a high temporal and/or spatial resolution without increasing operational costs.

Traditionally, phytoplankton is monitored by measuring chlorophyll *a* (chl *a*) concentrations, together with identification and counting of species under a microscope. Chl *a* is regarded as a proxy for total phytoplankton biomass (Steele 1962, Cullen 1982), although the amount of chl *a* relative to biomass is not constant (Jakobsen & Markager 2016), and it provides no information per se on community structure. The phytoplankton community is classically monitored by the Utermöhl technique (Utermöhl 1958), which includes species identification and cell enumeration and sizing using an inverted microscope. The main drawback of this widely employed method is time consumption, including time needed for sedimentation of samples plus time for microscopic analysis. Moreover, microscopic analysis demands experienced and skilled taxonomists. Also, considerable variability is found between taxonomists analysing the same sample (Jakobsen et al. 2015). Although inter-calibration efforts are routinely done (i.e. BEQUALM, and the Baltic Marine Environment Protection Commission–Helsinki Commission [HELCOM]), these results are usually only found as grey literature (Dürselen et al. 2014), and the ability to address complex assemblages of many species is not tested (Culverhouse et al. 2014). In addition, microscopic analysis requires samples to be fixed, a process which may cause cell deformation and loss, resulting in some species being impossible to identify and/or count (Hasle 1978, Choi & Stoecker 1989, Jakobsen & Carstensen 2011).

More recent monitoring techniques supplementing traditional monitoring include pigment measurements using HPLC, identification using molecular probes or analysing environmental DNA, and particle counts using flow cytometry, yet none of these methods has been widely employed for phytoplankton monitoring. Standard flow cytometry is largely employed in microbiology (Amann et al. 1990, Vives-Rego et al. 2000) for enumerating pico- and nanophytoplankton (Marie et al. 1997, Veldhuis & Kraay 2000, Tarran et al. 2006); however, this method is not suitable for analysing larger organisms. Image-in-flow cytometers are used to analyse larger organisms in a continuous mode, combining principles of flow cytometry and high-quality imagery (Sieracki et al. 1998, Olson & Sosik 2007). Such methods have fast analysis capability and the possibility for taxonomic identification; however, they have a restricted size range and are not suitable for analysing an entire phytoplankton community in a single run (Álvarez et al. 2011, Camoying & Yñiguez 2016, Dashkova et al. 2017).

Pulse-shape recording flow cytometry (PFCM) is a special type of flow cytometry suitable for analysing an entire phytoplankton community structure due to its broad size spectrum (1–800 µm) (Dubelaar et al. 2004). It has the ability to fingerprint individual cells by pulse shape profiles (Dubelaar et al. 2004), as opposed to standard flow cytometers (Thyssen et al. 2014, 2015). Note that in some publications, this technique has also been referred to as scanning flow cytometry, but because PFCM differs from scanning flow cytometry (Soini et al. 1998, Shvalov et al. 1999), we use the current terminology. The advantage of PFCM is that it is a fast (each sample can be enumerated in a few minutes) and relatively inexpensive method to process *in vivo* samples without the use of a fixative. This gives the method a promising potential in standard phytoplankton monitoring and in research projects, and is available as automated and benchtop versions. The PFCM can be connected with a camera for imaging and further identification of larger cells (Dugenne et al. 2014, Thyssen et al. 2015). However, the introduction of the technique in phytoplankton monitoring remains pending, awaiting the development of standardisation and comparison with other methods. A part of a wider acceptance of PFCM is exploring how PFCM data compare to those from traditional phytoplankton-monitoring techniques, i.e. does PFCM represent a promising future substitute or supplement to chl *a* and microscopy analysis?

The objective of this study is to compare standard methods such as chl *a* extraction and microscopic analysis with PFCM, using natural phytoplankton communities across a salinity gradient and seasons, thus representing a diverse range of communities. We hypothesise that specialised cell profile signals provided by PFCM can be used as a proxy for cell volume. In addition, we aim to: (1) compare results obtained by traditional methods and PFCM in terms of total biomass and community size structure, and

(2) assess which additional information can be gained from PFCM in comparison to standard monitoring using microscopy.

MATERIALS AND METHODS

PFCM

We used a desktop CytoSense (www.cytobuoy.com) PFCM, designed to address the complexity of natural phytoplankton communities. CytoSense can analyse a whole phytoplankton community, recording individual optical characteristics within minutes, although the exact analysis time is dependent on the sample (e.g. sample density and community composition) and equipment setup (e.g. flow rate, analysed volume—which typically varies from hundreds of µl to several ml). Briefly, phytoplankton cells are aligned by a sheath fluid before the cell travels across a 5 µm laser sheet (488 nm) (Fig. 1a). A trigger level determines the detection limit and can be set to reduce the number of non-target particles recorded in the data set, by ignoring cells with signals below the trigger level. A series of optical pulse-shaped signals are recorded as the cell travels through the laser sheet, creating a computer-generated silico image of the particle profile (Fig. 1b). These profiles reflect cell morphology and are to some extent species-specific and thus can be used to separate taxa at lower taxonomic levels. The equipment is sensitive enough to separate some of the recorded taxa into different physiological states (i.e. dividing and/or dying cells), and assigning them as separate clusters (Takabayashi 2006, McFarland et al. 2015). Furthermore, based on default algorithms, this PFCM technique allows particle length to be easily determined for all cells exceeding the width of the laser sheet. However, it is important to highlight that cells <5 µm are recorded by the optical sensors and that their integrated signal amplitude will be proportional to their volume. This allows distinction of smaller cells, provided that the cell produces a signal exceeding the pre-set trigger level. However, their precise length determination requires the use of other algorithms (McFarland et al. 2015) or calibration beads (Thyssen et al. 2008). The current PFCM is equipped with red (FLR; emission: 650–700 nm), orange (FLO; emission: 600–650 nm), and yellow (FLY; emission: 550 nm) fluorescence sensors. In addition, the instrument is equipped with side (SWS) and forward scatter (FWS) sensors that record light scattered orthogonally and parallel to the incident laser beam, respectively. The large size range among phytoplankton cells (0.5 to >1000 µm) produces signal intensities varying over several orders of magnitude. Therefore, the instrument is equipped with duplicate pairs of all sensors (except for the FWS): 1 standard (for large cells) and 1 high-sensitivity (for smaller nano- and pico-sized cells) sensor, allowing the instrument to cover the full size range of phytoplankton cells. As an example, the red fluorescence sensor is configured in 2 versions, namely FLR (normal sensitivity) and FLR-hs (high sensitivity). In addition, this PFCM is equipped with a camera that was set up to take photos of a random subset of the analysed particles (a limit of 150 pictures per sample was set in this study), which were used to support further identification.

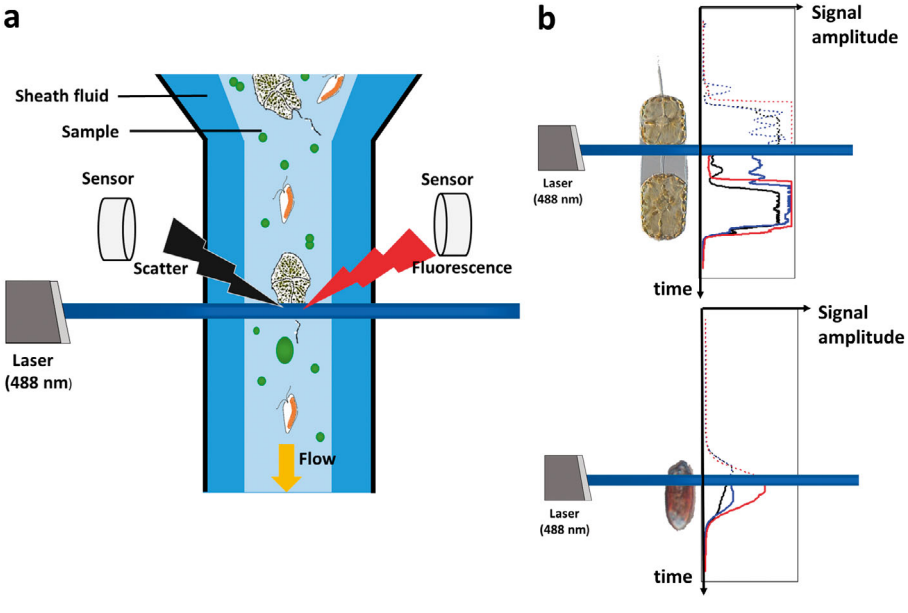

Fig. 1. Operating principle of CytoSense pulse-shape recording flow cytometer. (a) Particles oriented in their longitudinal dimension in the sheath fluid are excited by the blue laser beam and emit fluorescence and scattered light, which are recorded by different sensors. (b) Examples of integrated optical profiles are shown for 2 different phytoplankton species (*Ditylum brightwellii* [top graph] and *Rhodomonas* cf. *baltica* [bottom graph]) using red fluorescence (red line) and forward (black line) and sideward (blue line) scatter. As the cell travels through the laser beam, optical properties are recorded for each part of the cell, reflecting the general cell morphology. Adapted from www.cytobuoy.com

Volume calibration

Considering that the scatter signal in CytoSense is related to the cell size, it is likely that the integrated signal, recorded as the cell travels through the laser, reflects cell volume. To confirm this hypothesis and to derive a volume-conversion factor from integrated FWS signal to volume (µm^3), live cells from cultures of 18 different species (*Chroococcus* sp., *Coscinodiscus granii*, *Ditylum brightwellii*, *Dunaliella tertiolecta*, *Emiliania huxleyi*, *Gymnodinium aureolum*, *Isochrysis galbana*, *Isochrysis* sp., *Karlodinium veneficum*, *Micromonas pusilla*, *Pentapharsodinium dalei*, *Polarella glacialis*, *Prorocentrum micans*, *Prorocentrum minimum*, *Prymnesium patelliferum*, *Pyramimonas parkeae*, *Pyramimonas tychotreta*, and *Rhodomonas* cf. *baltica*), covering a size range from ~1 to ~125 µm, were measured under an inverted size-calibrated microscope (Nikon TI-U). In addition, commercial spheres ranging from 0.8 to 90 µm (0.8, 1.0, 2.9, 6.4, 15, 50, and 90 µm) were examined to test if these solid spheres had a significantly different optical behaviour than the phytoplankton cells. For information on the cultures and spheres, please see Table S1 in the Supplement at www.int-res.com/articles/suppl/a080p77_supp.pdf.

Based on microscopic measurements of the cells, the volumes of each species were calculated using recommended shapes from the literature (Hillebrand et al. 1999, Sun & Liu 2003). Total FWS and SWS of the silico images (profiles) in PFCM were integrated per cell for comparison between integrated scatter and volume. The number of measured cells under the microscope varied from 20 to 50 for each taxon, according to culture density, and because the PFCM recorded more cells, the same number of cells was randomly subsampled using the open-source statistical software R (R Core Team 2015). In the case of the spheres, volume was calculated based on the nominal diameter of the spheres given by the manufacturers assuming complete spherical shapes (see Table S1 in the Supplement for details).

The FWS signal was a better descriptor for volume than SWS, and only results from FWS are detailed in this study (SWS relationship with volume is available in Fig. S1 in the Supplement). For each of the 18 cultures and 7 sphere sizes, integrated FWS of each particle was averaged and compared to the average of the measured volumes from microscopy (cultures) and the calculated volumes (spheres). A log-log linear relationship between FWS and volume (VOL) with uncertainty on both axes was estimated (e_{VOL} and e_{FWS}):

$$\log(VOL) + e_{VOL} = a_{type} + b * \log(FWS) + e_{FWS} \quad (1)$$

and it was tested if the intercept of the relationship (a_{type}) varied between cultures and commercial spheres. Further, potential proportionality between FWS and volume was investigated by testing if $b = 1$, where b is the slope. These analyses were carried out with PROC MODEL in the statistical software package SAS 9.3.

Application to natural samples

From early March to late September 2015, water samples were collected approximately every month at 4 stations (1 freshwater: Stn RF0; and 3 estuarine: Stns RF1 to RF3) in Roskilde Fjord (RF), Denmark (Fig. S2 in the Supplement), totalling 44 samples covering a broad span of salinity and nutrient concentrations (Staehr et al. 2017). The freshwater station (Stn RF0) was sampled in a stream, draining from a lake into RF. Water samples (2 l) for phytoplankton measurements were taken from the surface (all stations) and at 4 m depth (estuarine stations only), brought to the laboratory, and analysed or fixed in acidic Lugol's solution (2–4% final concentration) within 1–4 h after sampling. On some occasions, it was not possible to perform the sampling: at Stn RF0 in late March, May, and June due to an absence of streamflow, and deeper samples (4 m) at the boundary station (Stn RF3) in July and August due to bad weather conditions.

Chl *a* was determined according to the method described by Strickland & Parsons (1972). Briefly, seawater (150–800 ml, depending on the filter colour) was filtered using GF/F filters, and chl *a* was extracted from the filter using ethanol (96%) during 24 h in the dark. The extracts were kept in a −20°C freezer until measured with an AU 10 Turner field fluorometer (Turner Designs), equipped with a lamp exciting at 450 nm and a filter collecting light emission at 670 nm.

Samples for the microscopic analyses were estimated under a size-calibrated inverted microscope (Nikon TI-U) following Hasle (1978). The samples were sedimented in Utermöhl chambers (Utermöhl 1958). The sediment chambers used ranged in volume from 2 to 50 ml according to cell density. Larger organisms, including ciliates (>30 µm), were usually screened under lower magnification (100×) and the screened area depended on the density of the most abundant organisms, whereas smaller organisms (<30 µm) were counted under higher magnification

(200× and 600×). In order to compare the phytoplankton size spectra from microscopy with that of the PFCM, cells were first identified to the lowest possible taxonomic level using different size intervals, and secondly grouped into 3 general size classes: pico- (<5 µm), nano- (5–20 µm), and microphytoplankton (>20 µm) based on the maximum linear diameter. The 5 µm threshold for picophytoplankton was chosen to investigate potential limitations with microscopy analysis, where cells <5 µm are not consistently recorded. PFCM is sensitive enough to record cells <5 µm, due to the optical sensors. It is important to emphasise that even cells <2 µm, such as *Synechococcus* and pico-eukaryotes, are recorded with the PFCM, as shown in previous studies (Bonato et al. 2015, 2016, Thyssen et al. 2015), but to obtain their lengths, other means need to be employed (see subsection 'PFCM' above for further details).

For the PFCM analyses, *in vivo* samples (500–1000 µl, at a flow rate of 8 µl s^{-1}) were analysed in triplicate using the software CytoUSB (www.cytobuoy.com) and FLR-hs set at 30 mV as a trigger, to ensure that only cells containing chl *a* were recorded. For comparison with microscopy, cells were clustered according to their optical properties (similar to the taxonomic identification using the microscope), and the statistical properties of the clusters were calculated, before the clusters were grouped into the 3 general size classes. Cluster definitions were made with help of the software CytoClus3 (www.cytobuoy.com) by visualising the data in multiple scatterplots on different optical properties (length and total FWS, total FLR, total FLO, total SWS) using the mutually exclusive option, i.e. cells were assigned to 1 cluster only. Clusters were determined manually for each sample, based on particle optical similarity on the different scatterplots (see Fig. S3 in the Supplement for an example), and the cluster gating and order was always the same within a sample station. Clustering was further supported by examining individual optical profiles and photos of analysed particles, when available. Signals (mV) from the FWS, FLR, and FLR-hs were integrated for each cell and subsequently for each sample, expressing total FWS and red fluorescence (note that those parameters were normalized by the analyzed volume of each sample). Average cell length given by the FWS signal for the particles in each cluster was used to classify the different clusters into the same general size classes as used for microscopy. The chains were split into separate cells using the software-specific algorithm ('cell counts for chain-forming particles'), in order to make the cell counts more comparable with microscopy.

Carbon biomass

For the microscopic analyses, carbon biomass was estimated from cell volumes. For each taxon, 20–50 specimens were analysed using the same protocol as in the 'Volume calibration' subsection above. The volume estimate was made for each taxon and size class (some taxa scaled over several size classes) in each location (but were not done systematically for each sampling time and depth), and the average cell volume from the subsample was subsequently used for all counts of the taxon and size class.

For the PFCM analyses, cell volume was calculated from the integrated FWS per cell using the established relationship from the 'Volume calibration' experiment above, according to Eq. (1).

For both methods, cell volume was converted to carbon biomass using a generic protist formula (Menden-Deuer & Lessard 2000). Cell volume and biomass were aggregated to the 3 general size classes (assignment was based on the average maximum linear diameter) for comparisons between microscopy and PFCM.

Method comparison

Relationships between chl *a* and red fluorescence of the PFCM (FLR and FLR-hs) were investigated using the following empirical model:

$$\log(\text{chl } a) + e_{\text{chl } a} = a_{\text{station}} + b_{\text{layer}} + c_{\text{month}} + d^{\star}\log(\text{FLR}) + e_{\text{FLR}} \quad (2)$$

where a_{station} was a factor describing differences between the 4 stations, b_{layer} was a factor describing differences between surface and deeper samples, and c_{month} was a factor describing differences between months of sampling, d is the slope of this relationship and e is the error term associated with the model. Thus, these 3 factors described station-specific, layer-specific, and month-specific scaling factors in the power relationship derived from the model, and these factors were used to test the generality of the relationship, i.e. if the intercept of the log(chl *a*)-log(FLR) relationship varied between stations, layers, and months. Both FLR and chl *a* were associated with an error term. Model reductions were analysed using the likelihood ratio (LR) test by imposing constraints on the parameters, i.e. using 4 station-specific parameters for the stations versus using 1 general parameter, and so forth for layers and months. Model reductions were carried out iteratively by removing the least significant term first. The

log-log relationship (Eq. 2) corresponds to a power relationship on the original scale, and the proportionality between FLR and chl *a* was tested with the parameter constraint $d = 1$.

Similarly, cell densities and carbon biomass estimated from the PFCM were compared to the values obtained from the microscope analyses. For these analyses, the same type of model as above (Eq. 2) was employed, i.e. uncertainty was associated with both methods, for the 3 size classes separately (<5, 5–20, and >20 µm) to investigate potential differences. If the 2 methods indeed produced similar results, a consistent proportional relationship ($d = 1$), invariable to sampling time and location, was expected with a common intercept of 0, corresponding to a scaling factor of 1 on the original scale. The invariability of the relationship to sampling time and location as well as the proportionality of the relationship was tested with the LR test by imposing parameter constraints on $a_{station}$, b_{layer}, and c_{month}. All analyses were carried out with PROC MODEL in the statistical software package SAS 9.3.

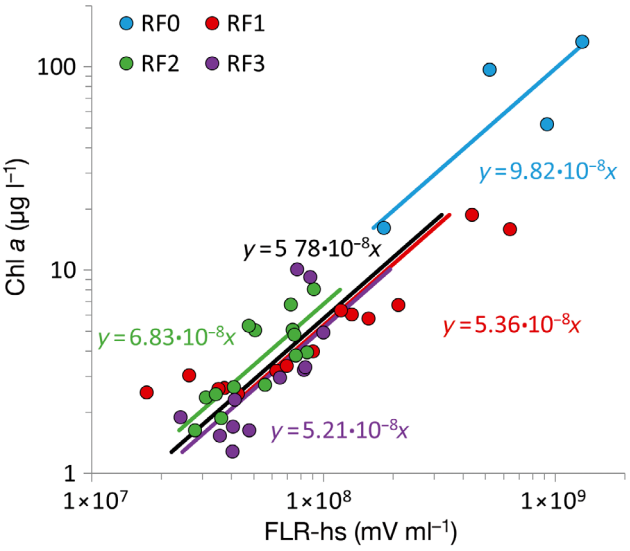

Fig. 2. Total high-sensitivity red fluorescence (FLR-hs) versus chl *a* concentrations sampled at 4 different stations in Roskilde Fjord. The common relationship for the 3 estuarine stations (Stns RF1, RF2, RF3) is shown in black. Stn RF0 is freshwater

RESULTS

Sampling was conducted over the main productive period, with temperatures ranging from ~3°C in March to ~18°C in August at all stations. Salinity increased from the freshwater station (Stn RF0) to ~15 at Stn RF1, ~20 at Stn RF2, and ~22 at Stn RF3, with a tendency to larger seasonal fluctuations at the outer stations. Differences in salinity and temperature between surface and 4 m samples were small, confirming that the water column in RF is mostly well mixed throughout the season (Staehr et al. 2017).

Chl *a* versus total red fluorescence

Total fluorescence from the FLR-hs sensor in Eq. (2) yielded a better description of the observations than using the normal FLR sensor and was consequently used in the following analysis. The errors associated with total FLR-hs and chl *a* were of similar magnitude, corresponding to a relative uncertainty of 52% and 45% (0.42 and 0.37 on the log-scale), respectively. No significant difference between estimates based on total chl *a* and FLR-hs was found between surface and deeper samples (LR = 0.00, p = 0.9880) or between months of sampling (LR = 3.27, p = 0.6584), whereas there was a significant difference between the 4 stations (LR = 9.81, p = 0.0203). The relationship was not significantly different from proportionality (i.e. $d = 1$; LR = 1.48, p = 0.2245). The significant variation among stations was not changed (LR = 9.46, p = 0.0237) after reducing the model (Eq. 2) by removing non-significant factors ($a_{station}$ and b_{layer}) and setting $d = 1$. But the variation was mainly driven by the freshwater station deviating from the estuarine stations (Fig. 2). In fact, there was no significant difference between the 3 estuarine stations (LR = 3.49, p = 0.1743), yielding an estuarine conversion factor from total FLR-hs to chl *a* of 5.78×10^{-8}, whereas the conversion factor for the freshwater station was 9.82×10^{-8}.

Applying the empirical formula above (Eq. 2) makes it possible to extract an estimate of the chl *a* contribution of the different clusters or size classes from PFCM. For the present data set, we estimated chl *a* for the general size classes using the conversion factors in the previous paragraph (Fig. 3). The sums of the estimated values were generally in agreement with the extracted chl *a* values, although with some differences. At Stn RF0, the estimated chl *a* concentration in March and July matched the extracted chl *a* values, although lower and higher estimated chl *a* compared to the extracted values were found in August and September, respectively (Fig. 3a). At Stn RF1, discrepancies between estimated and extracted chl *a* were found in late March and July, being more pronounced in the former (Fig. 3b). In

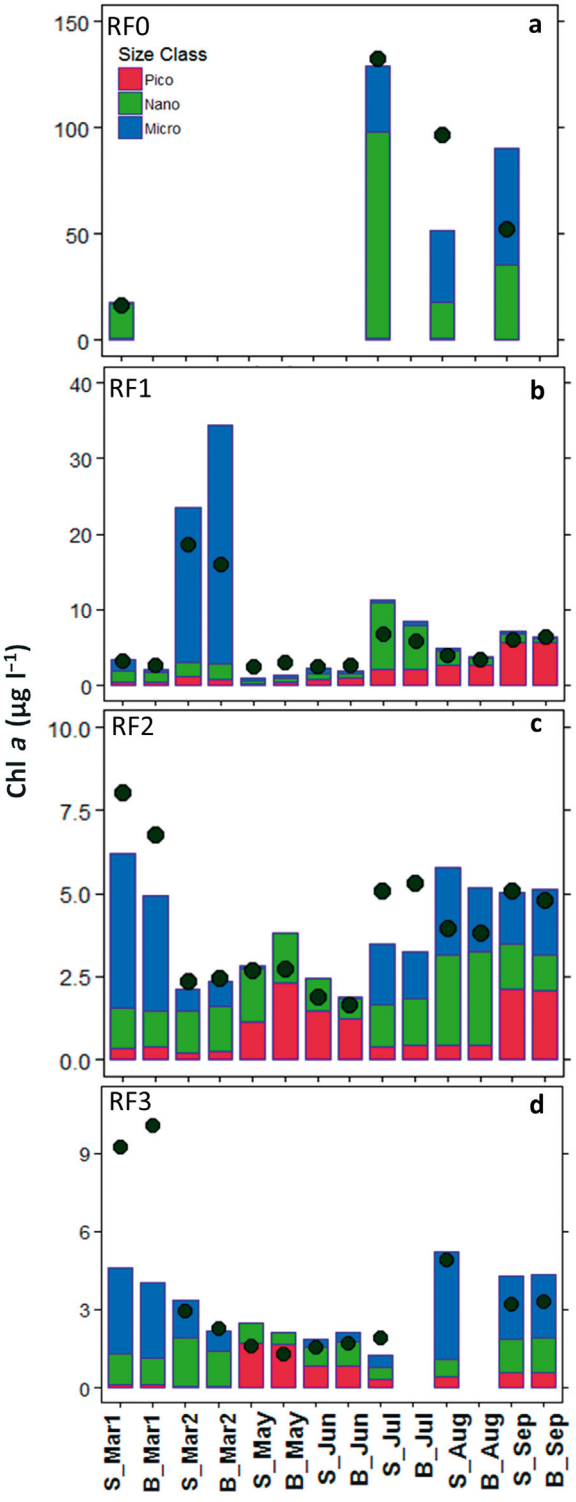

Fig. 3. Total extracted chl *a* (●) and chl *a* estimated from high-sensitivity red fluorescence (FLR-hs) measured by pulse-shape recording flow cytometry separated into 3 size classes of phytoplankton (coloured bars) for the 4 stations (panels a to d: Stns RF0 to RF3). Each symbol and bar represent 1 sample from different months (Mar1: early March, Mar2: late March) and layers (S: surface, B: bottom)

late March, differences between the surface and 4 m depth were more noticeable for the estimated than extracted chl *a*, with higher and lower values relative to the surface found for the estimated and extracted chl *a*, respectively (Fig. 3b). Stn RF2 presented differences in March, July, and August, but for those months the differences between extracted and estimated chl *a* were small (Fig. 3c). At Stn RF3, estimated values were close to the extracted ones, except in March, when extracted values were about 2 times higher than the estimated ones (Fig. 3d). The size-fractionated chl *a* estimated by the PFCM indicated that smaller phytoplankton (pico- and nanophytoplankton) were important at all estuarine stations, especially in May–June at Stns RF2 and RF3 (Fig. 3c,d) and summer at Stn RF1 (Fig. 3b).

Cell density comparison

Cell densities from microscopy and PFCM were comparable for micro- and nanophytoplankton (Fig. 4a,b), whereas picophytoplankton cell densities were substantially higher when measured with the PFCM (Fig. 4c).

For microphytoplankton, there were no systematic differences between depths (LR = 0.00, p = 0.9764) or among stations (LR = 5.68, p = 0.1285). Furthermore, proportionality between the 2 methods could be assumed (i.e. $d = 1$; LR = 2.48, p = 0.1152), but there were significant differences among months (LR = 72.96, $p < 0.0001$). However, the variation in the scaling factor among months was entirely driven by the samples from May, yielding significantly higher PFCM cell densities than from microscopy, whereas differences among the other months were not significant (LR = 4.61, p = 0.4652). Consequently, with the exception of May, there was proportionality between cell densities obtained from microscopy and PFCM scaling by a factor of 0.96 (Fig. 4a), which was not significantly different from 1 (LR = 0.10, p = 0.75436).

For nanophytoplankton, there was no systematic variation between layers (LR = 0.41, p = 0.5243), and proportionality between the 2 methods could be assumed (i.e. $d = 1$; LR = 1.26, p = 0.2626), as well as the scaling factor that was not significantly different among stations (LR = 5.46, p = 0.1410) or months (LR = 6.11, p = 0.2960). Consequently, a simple log-log relationship between the 2 methods was estimated with a scaling factor of 1.08 (Fig. 4b) that was not significantly different from 1 (LR = 0.52, p = 0.4720) (Fig. 4b).

For picophytoplankton, the difference between layers was the least significant (LR = 0.33, p = 0.5634),

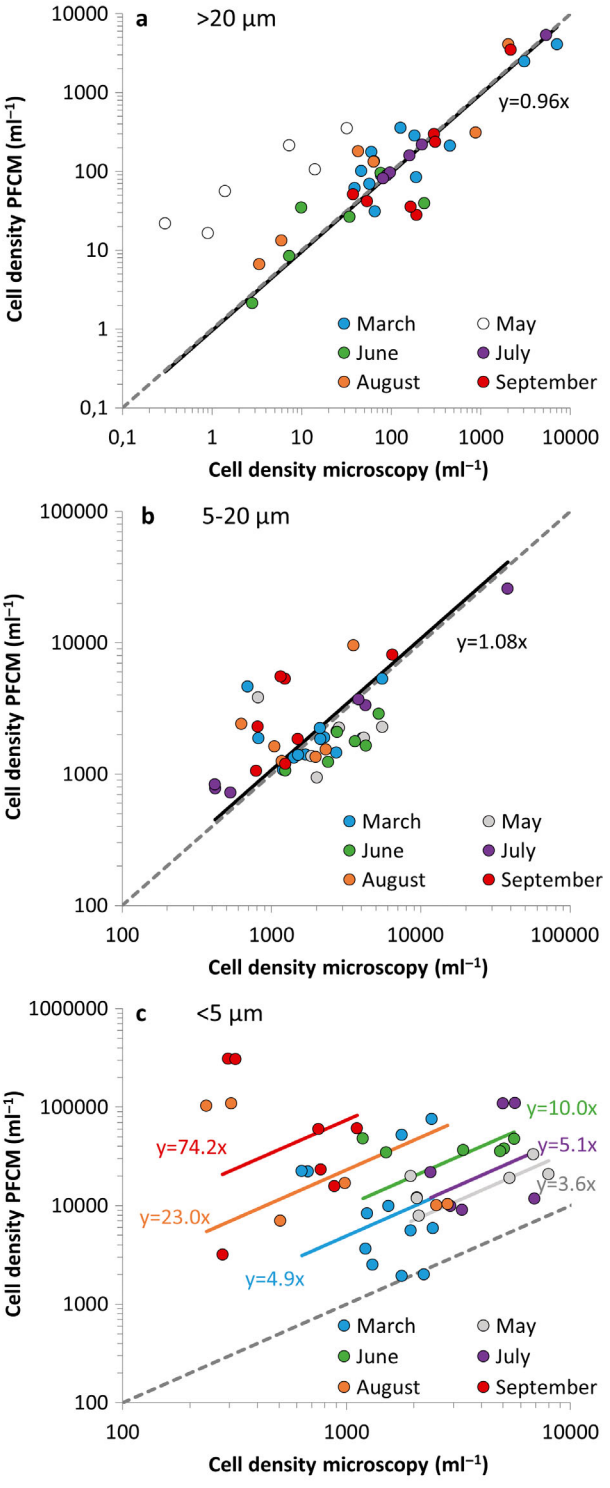

Fig. 4. Comparison of cell densities measured by microscopy and pulse-shape recording flow cytometry (PFCM) for the 3 general size classes of phytoplankton (a: >20 µm, b: 5–20 µm, c: <5 µm). The estimated log-log linear relationship with uncertainty of both axes (black solid line) is compared with the identity line (dashed grey line). For picophytoplankton (<5 µm), estimated relationships are shown for each month using the same colour code as for the symbols

followed by the slope of the log-log relationship (LR = 2.58, p = 0.1080). However, systematic differences were found among stations (LR = 63.99, p < 0.0001) and months (LR = 64.18, p < 0.0001), suggesting that the 2 methods differed for almost every sample. Differences were particularly pronounced for August and September at all stations (Fig. 4c), as well as for all months at Stn RF1 (data not shown). Averaged over the stations, cell densities from PFCM were 23 and 74 times higher in August and September, respectively, whereas cell densities from the PFCM were ~5–10 times higher for the other months. Averaged over months, cell densities from the PFCM were ~60 times higher at Stn RF1, in comparison to ~5 times higher at the other stations (data not shown).

The differences between the 2 methods were apparent in terms of size distributions (Fig. 5). Whereas the PFCM-measured cell density generally decreased exponentially with the maximum length dimension, the cell densities of picophytoplankton (<5 µm) from microscopy were in many cases similar to or even lower than phytoplankton within the 5–10 µm range, yielding a different size distribution for the smallest phytoplankton. The size distributions of the 2 methods appeared to match reasonably within the nanophytoplankton scale (5–20 µm). For larger size ranges, it was challenging to compare the 2 methods due to the relative discrete nature of cell density from microscopy (microphytoplankton size classes from microscopy were broader, while in PFCM they were defined for each 1 µm). The size distribution varied broadly among stations, with the smallest cells (on average) at Stn RF1 and larger cells at Stn RF0, as well as that larger cells were more frequent in September compared to the spring populations.

Cell volume comparison

Calculating carbon biomass from PFCM was based on calibrating total cell FWS to microscopically determined cell volumes (Eq. 1), before applying volume-carbon biomass relationships. Volumes of the cultured cells and commercial spheres spanned 6 orders of magnitude (Fig. 6). There was no significant difference in the scaling between volumes of cultured cells and spheres (LR = 0.06, p = 0.8082), but the slope of the log-log relationship was significantly different from 1 (LR = 192.61, p < 0.0001), yielding a progressively increasing cell volume with total cell FWS. Hence, total cell FWS does not scale proportionally to cell volume, resulting in a ratio between total cell FWS and cell volume that gradually levels out for larger cells.

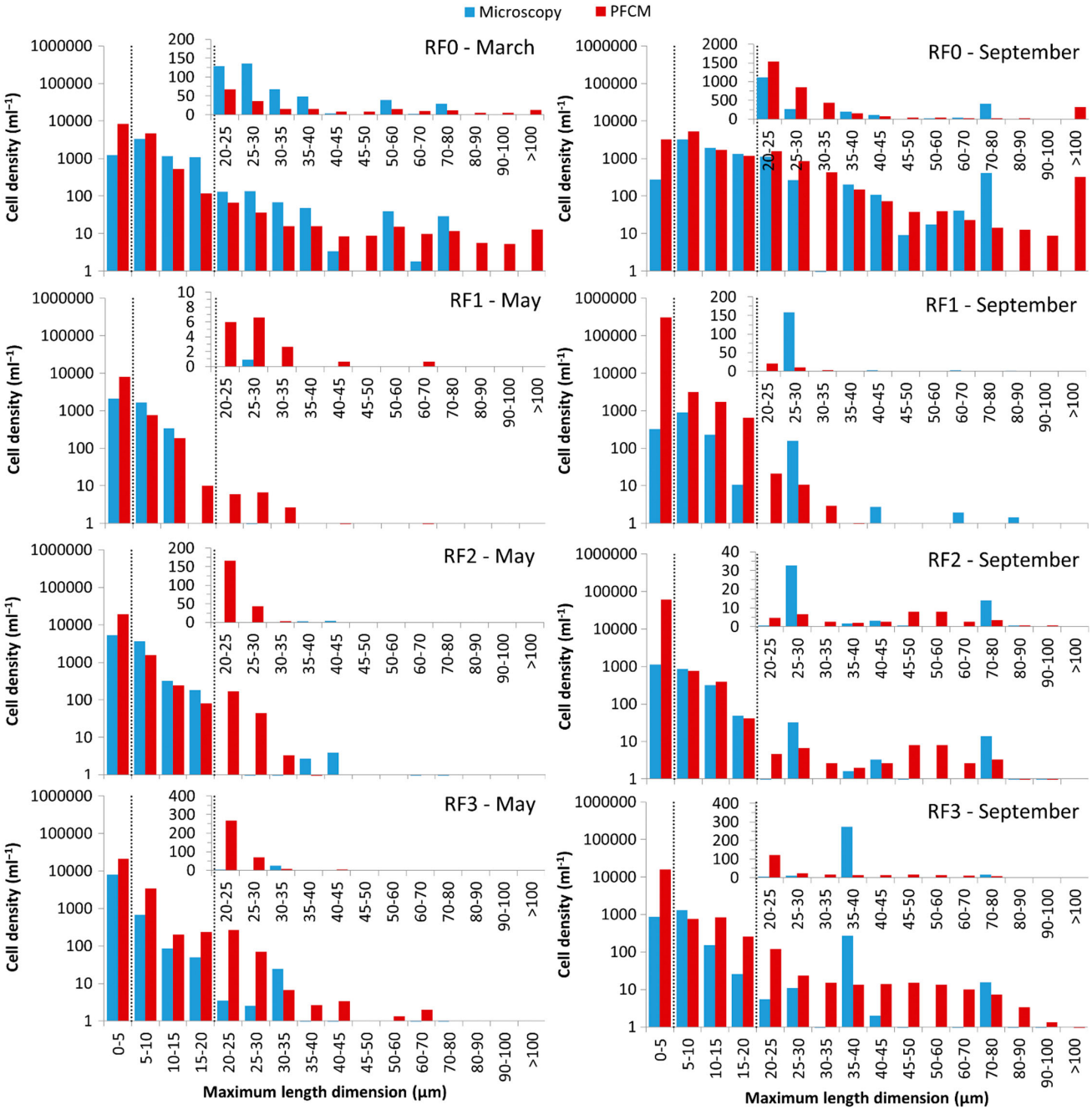

Fig. 5. Comparison of phytoplankton size distributions from microscopy and pulse-shape recording flow cytometry (PFCM) at the 4 stations (top to bottom: Stns RF0 to RF3) with the month of the most similar distribution to the left and the month of the most dissimilar distribution to the right (surface samples only). For Stn RF0, no sample was taken in May and therefore the March sample was used. Size distributions for the entire population are shown on log-scale, with the microphytoplankton size distribution on the raw scale shown as inset in each plot. Vertical dotted lines indicate cell sizes for separating micro-, nano-, and picophytoplankton. Note the different *y*-axis scales for the inset graphs

Community carbon comparison

For microphytoplankton community carbon, the variation in community carbon biomass between PFCM and microscopy was not significant between depths (LR = 0.07, p = 0.7854) or among months (LR = 4.39, p = 0.4945) or stations (LR = 4.53, p = 0.2094) (Fig. 7a). The scaling factor was not significantly different from 1 (LR = 1.66, p = 0.1970), but the slope of the log-log relationship was significantly different from proportionality (i.e. d = 1, LR = 19.71, p < 0.0001). This implied that carbon biomass estimates

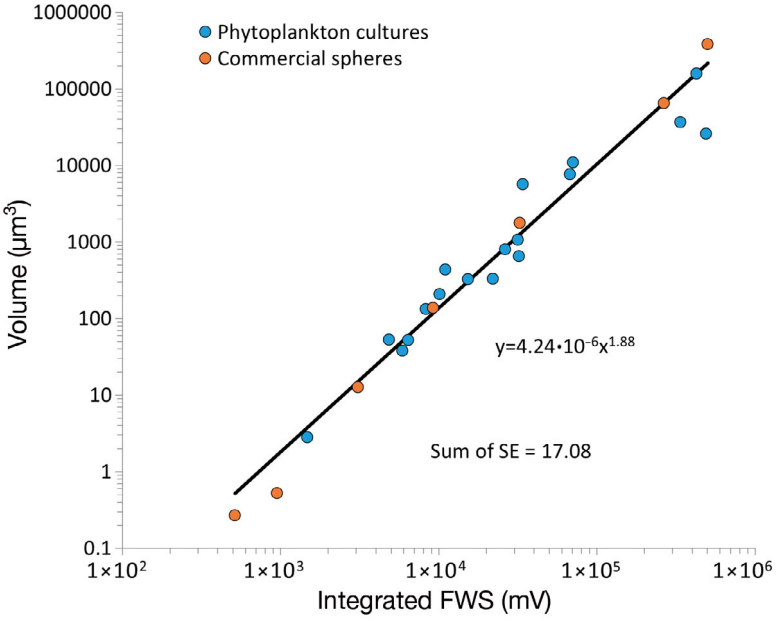

Fig. 6. Calibration relationship for average volumes of 19 phytoplankton cultures (Table S1 in the Supplement; measured by microscopy) and 7 commercial spheres (calculated volume from diameter) versus average integrated forward scatter (FWS) measured with pulse-shape recording flow cytometry

were similar for the 2 methods at low values, whereas PFCM gave generally higher carbon biomass estimates at high values (Fig. 7a), deviating by up to a factor of 3 across a carbon biomass range of 4 orders of magnitude. Random variation around the regression line was 1.16 and 1.02 on the log-scale, corresponding to a relative uncertainty of 220% and 177%, for PFCM and microscopy, respectively.

For nanophytoplankton, the slope of the log-log regression between PFCM and microscopy was not significantly different from proportionality (i.e. $d = 1$, LR = 0.03, p = 0.8659), and variation between depths was not significant (LR = 0.23, p = 0.6287). However, there were significant differences among months (LR = 12.42, p = 0.0295) and stations (LR = 16.40, p = 0.0009), yielding scaling factors ranging between 1.66 and 4.58 for months (Fig. 7b) and between 1.44 and 5.59 for stations (highest for Stn RF0 and lowest for Stn RF2). All scaling factors were >1, resulting in generally higher carbon biomass with the PFCM method. Random variation around the regression line was smaller than for microphytoplankton with a relative uncertainty of 90% (0.64 on the log-scale). The values and range in nanophytoplankton carbon biomass were smaller than for microphytoplankton.

For picophytoplankton, the variation between depths was not significant (LR = 0.11, p = 0.7398), and proportionality between PFCM and microscopy could be assumed (i.e. $d = 1$, LR = 2.64, p = 0.1041). However, the proportionality between methods scaled by factors that varied significantly among stations (LR = 17.94, p = 0.0005) and months (LR = 48.80, p < 0.0001). Scaling factors for stations ranged from 15.6 at Stn RF3 to 52.5 at Stn RF1, whereas scaling factors for months ranged from 6.2 in March to 79.3 in September (Fig. 7c). Picophytoplankton community carbon biomass was low compared to micro- and nanophytoplankton community carbon biomass, ranging across 2 orders of magnitude. The relative uncertainty around the regression lines was 121% (0.7939 on the log-scale). Community carbon biomass estimates with PFCM were consistently higher than the microscopy samples.

For total phytoplankton community carbon biomass, differences between methods for the 3 size groups partially evened out to provide a simple proportional relationship with a scaling factor of 2.53 (Fig. 7d). Variation between depths was not significant (LR = 0.08, p = 0.7791), and the slope of the log-log relationship was not significantly different from 1 (LR = 0.88, p = 0.3483). Variations among months (LR = 6.27, p = 0.2812) and stations (LR = 5.44, p = 0.3650) in community carbon biomass were also not significant. However, the resulting scaling factor of 2.53 was significantly different from 1 (LR = 56.03, p < 0.0001). The relative uncertainty was 126%, a compromise between the high uncertainty of microphytoplankton and those of nano- and picophytoplankton. It was noteworthy that the progressively increasing relationship for microphytoplankton (i.e. $y = x^{1.14}$) was balanced by higher carbon biomasses with the PFCM for nano- and picophytoplankton to provide a simple proportional relationship between the 2 methods (Fig. 7).

DISCUSSION

This study compared PFCM-derived information with extracted chl *a*, microscopy counts, and carbon estimates, which are traditionally used in monitoring and research projects. We demonstrated that total FLR from PFCM is well correlated with extracted chl *a*, and that a conversion factor from this relationship allows the conversion of FLR to chl *a* concentration on the population and on the community levels.

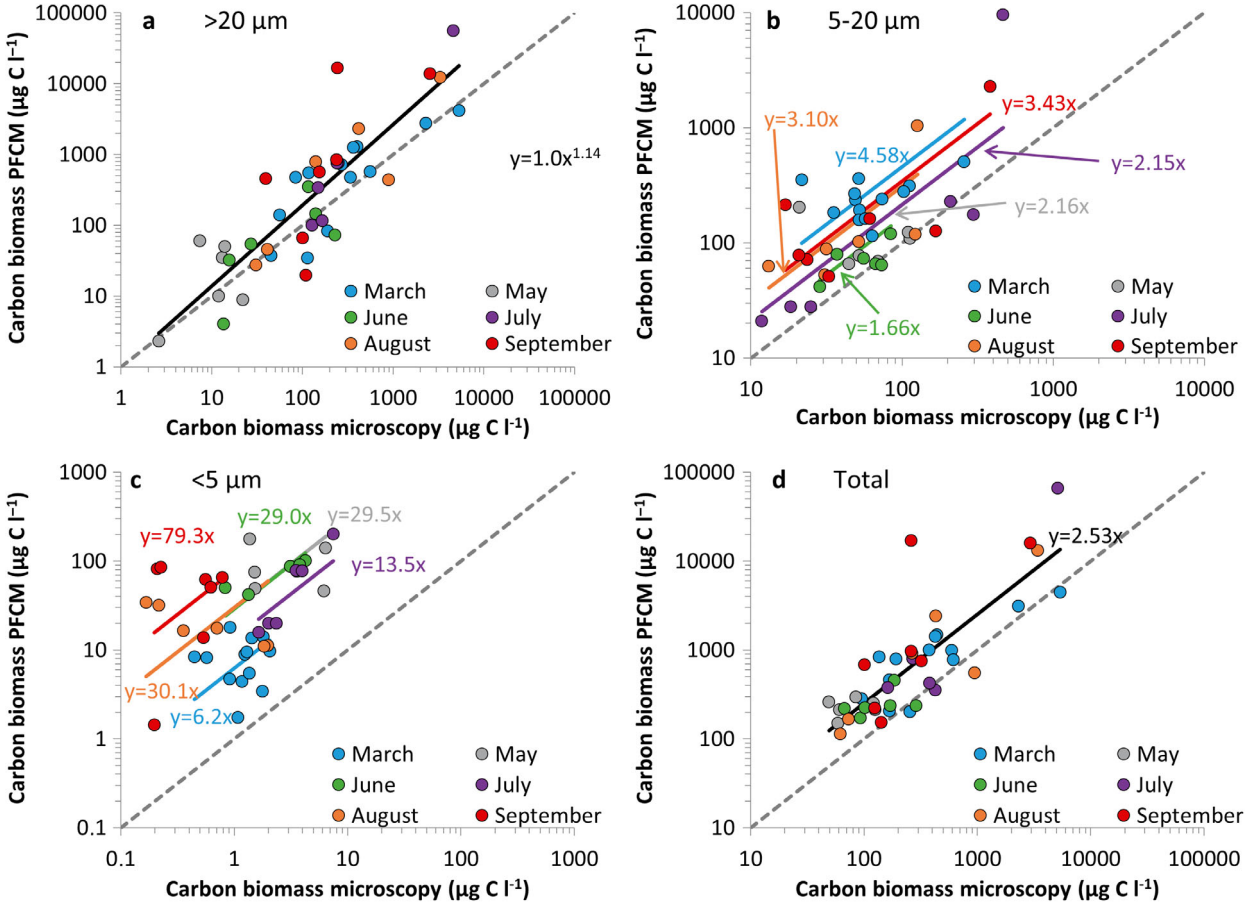

Fig. 7. Comparison of carbon biomass estimated from microscopy and pulse-shape recording flow cytometry (PFCM) for (a) micro-, (b) nano-, (c) pico-, and (d) all phytoplankton. Dashed grey line marks the identity line. For nano- and picophytoplankton, estimated relationships are shown for each month (mean across all 4 stations) using the same colour code as for the symbols, whereas for microphytoplankton and total carbon biomass, differences between stations, layers, and months were not significant and the simple log-log linear relationship (solid black line) is shown

We also showed that cell counts from PFCM are comparable with cell counts from light microscopy for cells >5 µm. Furthermore, we showed that PFCM is able to analyse cells <5 µm, which are not properly counted in light microscopy. This leads us to propose a method to estimate volumes of individual live cells from total FWS across the full size range of phytoplankton encountered in natural communities.

Chl *a* and total red fluorescence

Overall, there was good agreement between total community chl *a* estimated by PFCM and extracted chl *a* (Fig. 3). Differences between methods found in some samples are unlikely due to the lamps and filter sets used in the fluorometer (excitation at 450 nm and emission at 670 nm) and PFCM (excitation at 488 nm and emission at 650–670 nm), which are similar. Discrepancies could be explained partly by the community composition, as high concentrations of colony-forming organisms and large diatoms (i.e. *Chaetoceros* spp., Rhizosoleniaceae, *Dolichospermum*, *Microcystis*, and *Aphanizomenon*; Table S2 in the Supplement) were observed in almost all samples with disagreement between extracted and PFCM-estimated chl *a* (Fig. 3a,c,d). Colony-forming organisms and large diatoms may result in higher particle heterogeneity of the sample, increasing the variation within the relatively small sample volume analysed by PFCM. However, discrepancies between the 2 methods were consistent for both surface and bottom samples (Fig. 3), suggesting that discrepancies between the 2 methods were caused by factors other than increased variability due to larger particles. Instead, the difference between the 2 methods could be due to differences in community composition and environmental factors influencing *in vivo* fluorescence

(measured as FLR-hs in this study) and extracted chl *a* differently (Kiefer 1973, Lutz et al. 2003). Cell-specific fluorescence by PFCM reflects a combination of cell physiology and species-specific pigment composition and shading by packing of chloroplast in larger cells, which may yield lower fluorescence signals in the PFCM. In contrast, chl *a* in the cell is mainly regulated by availability of light and nutrients (Jakobsen & Markager 2016). This could be the cause of the discrepancy observed at Stn RF1, where higher chl *a* estimates from the PFCM were found in late March during the spring bloom. The spring bloom was dominated by *Eutreptiella* sp., and a visual inspection of live samples revealed that cells at 4 m depth appeared to be in a different physiological stage, with fewer dividing cells and loss of flagellae, than the cells collected at the surface. Most likely, this sample represents the later phase of the spring bloom, when nutrient limitation reduces chl *a* content in the cells and senescent cells sink from the surface layer. In comparison with the surface, the low chl *a* relative to PFCM fluorescence at 4 m depth supports the fact that the deeper community was in an ageing state.

The differences found in FLR-hs versus chl *a* scaling between the freshwater and estuarine stations (Fig. 2) could also be explained by differences in community composition and physiology of the cells. The phytoplankton community was dominated by cyanobacteria only at Stn RF0, and this group has distinct fluorescence characteristics, due to the presence of phycobiliproteins, and distinct physiology of photosystems I and II, with an imbalance of energy between them leading to different fluorescence and absorption spectra compared with other phytoplankton life forms (Campbell et al. 1998, Lutz et al. 2001). Chl *a* and phycobiliproteins found in cyanobacteria have different excitation-emission spectra that may partly overlap into the FLR-hs emission broader band (650–670 nm). Consequently, divergence between the 2 methods may arise when the cyanobacterial contribution is important. Similarly, low *in vivo* fluorescence relative to measured chl *a* has been reported for cyanobacteria-dominated communities (Pinto et al. 2001, Gregor & Maršálek 2004).

Despite differences, PFCM provides a good proxy for estimating total chl *a* in a sample within minutes, although pre-calibration with traditional chl *a* extracts may be required in order to obtain reliable conversion factors from FLR-hs to chl *a*. Moreover, PFCM enables a flexible chl *a* fractionation to separate a large number of size classes or even different parts of the phytoplankton community, provided that they can be discriminated in the clustering process. Importantly, this separation into different groups can be done after the sample has been analysed, i.e. the fractionation does not need to be determined beforehand.

Cell enumeration

For cell densities, noticeable differences between methods were found, particularly for the picophytoplankton size fraction. Both enumeration methods were comparable for micro- and nanophytoplankton, even considering the smaller analysed volume in the PFCM (500–1000 µl) in comparison to microscopy (2–50 ml). For microphytoplankton, cell density estimates of the 2 methods were comparable (Fig. 4a,b) and the differences were, in most of the cases, within the range of the expected counting errors. As an example, cell numbers counted with an inverted microscope varied by a factor of up to 3 for some species within the same sample counted in triplicate (Jakobsen 2012). The estuarine samples from May significantly differed from the other months (Fig. 4a), with higher PFCM cell counts than microscopy counts. May samples were also different in terms of community composition and size structure. At Stn RF1, this was probably due to a large number of ciliates and a low number of large phytoplankton cells in the May samples (the proportion of counted cells of microphytoplankton to ciliates, determined by inverted microscopy, were ~1:50 and ~1:80, at the surface and 4 m, respectively). Ciliates that have been feeding on phytoplankton can also trigger an FLR signal because of partly digested chloroplast or retained chloroplasts for mixotrophic nutrition and hence be recorded by the PFCM as phytoplankton, whereas they can be discriminated under the microscope. At Stns RF2 and RF3, the density of ciliates was lower than at Stn RF1, but microphytoplankton cells were not as abundant as in other samples. Additionally, most of those microphytoplankton cells ranged between 20 and 30 µm, close to the threshold between size classes, and could be placed differently into size classes when counted by the PFCM, because size-class assignment for PFCM was based on the clusters' average length.

Nanophytoplankton cell densities recorded by the 2 methods generally agreed, although differences could reach factors of 3 to 5 in some samples (Fig. 4b). For this size fraction, more detailed taxonomic information from the Utermöhl technique is limited due to a lack of cell movement observations as well as alterations in morphology and colour. Differences found

between months and stations for this size fraction could be explained by differences in the phytoplankton community composition, particularly when there were many small cells close to the picoplankton size. Picophytoplankton cell density was lower in the microscope analysis (Fig. 4c), probably because the optical limitations of light microscopy increased the risk of overlooking these small cells and because deformed cells can be more easily confounded with detritus. Thus, even though some cells <5 µm were counted in the microscope for this study, the entire picoplankton community was not counted. Phytoplankton cells <2 µm are generally not counted with the Utermöhl technique, but enumerated using epifluorescence or flow cytometry (Edler & Elbrächter 2010). Lugol's fixation, which was used in the sample preparation, also induces a bias by destroying and shrinking cells to various degrees, yielding lower cell counts when compared to *in vivo* counted cells as in PFCM (Choi & Stoecker 1989, Zarauz & Irigoien 2008, Jakobsen & Carstensen 2011).

The Utermöhl method remains the standard technique in today's monitoring programmes, because it also provides taxonomic information (Zingone et al. 2015). Apart from the fact that it is time-consuming and results depend on the taxonomist's skills (Jakobsen et al. 2015), in many cases, proper species identification requires the supplementation of other techniques, such as electron microscopy, epifluorescence, or molecular techniques (which are not always suitable to the monitoring format) (Zingone et al. 2015). Additionally, the fixation process can destroy or deform many organisms, making the counting biased towards larger and/or more resistant organisms (Choi & Stoecker 1989, Zarauz & Irigoien 2008, Jakobsen & Carstensen 2011).

Volume conversion from FWS

The volume conversion results showed a strong positive relationship between particle volume and total FWS (Fig. 6). Since cell size, shape, and biochemical composition influence the particles' refractive index and scattering properties (Stramski & Mobley 1997, Voss et al. 1998), it is expected that FWS depends on the type and characteristics of analysed particle. Solid beads are expected to have a higher refractive index than live phytoplankton cells, while presence of cell coverage of some species will increase light scattering. However, no significant differences were found between phytoplankton cells and spheres, and due to the diverse nature of the particles employed in this calibration, live phytoplankton cultures comprising different taxonomic groups with different cell coverage (e.g. organic scales, theca, silica frustule, and naked cells) and solid beads, all scaling over a broad size range, the particle-specific bias was reduced. It is important to highlight that this calibration is instrument-specific, depending on how the sensor's sensitivity is set from the factory. However, our results show that the relationship among FWS and cell volume does not change between phytoplankton cells and commercial polystyrene beads.

Biomass estimation and comparison

Carbon estimated for microphytoplankton showed changes in the slope, indicating that carbon estimates were higher for PFCM, especially for larger cells. Fixation induces cell loss and causes cell shrinkage. Because the carbon conversion factor is an exponential function, the shrinkage effect is more pronounced for larger cells than smaller cells. Community composition may also play an important role for the determination of carbon, as the samples with highest biomass values from PFCM had a larger contribution of *Chaetoceros* spp., *Rhizosolenia* spp., *Pseudosolenia calcar-avis*, *Microcystis*, and *Dolichospermum* spp. An overestimation of carbon by PFCM can occur (e.g. for *Chaetoceros* spp.), when the colonies are coiled and/or entangled, because they are recorded in PFCM as a single organism with an inflated volume due to the presence of setae. A similar behaviour is observed for samples with a high contribution of cyanobacteria with coiled trichomes or mucilaginous colonies. However, in samples with a high contribution of *Rhizosolenia* spp. and *Pseudosolenia calcar-avis*, carbon is likely to be underestimated using microscopy, because these cells are long and delicate and could easily be damaged by the homogenisation prior to the sedimentation. In such samples, we found a large number of broken cells that were not counted in microscopy.

For nanophytoplankton, higher community carbon biomasses from the PFCM can also be explained by the differences in analysis of live (PFCM) and fixed cells (microscope). It is important to stress that the recommended shapes for organisms in this size class are restricted to a few options that may also lead to a misrepresentation of their volume and biomass. For picophytoplankton, the difference in the community biomass estimate between methods is probably due to lower cell counts in microscopy.

The estimated phytoplankton community carbon biomass was about 2.5 times higher for PFCM than microscopy (Fig. 7d). This difference is partly due to the higher contribution of picophytoplankton counted by PFCM than by microscopy. However, the overall contribution of this size fraction to total is variable over time and can be very small when compared to nano- and microphytoplankton. Fixative was systematically used in all the microscope samples and it can be responsible for a reduction of 20 to 55% in cell volume in comparison with live samples (Choi & Stoecker 1989, Montagnes et al. 1994). Therefore, taxonomic changes in the community and the shrinking effect of the fixative are the main causes for the discrepancy between methods.

Monitoring and research implications

One of the main advantages of PFCM over traditional methods is the speed in which a sample can be analysed (about a few minutes) and further processed (when the value range of parameters is defined for the clusters and algorithms are written and working, the whole process takes <30 min). Moreover, training for PFCM operation demands less time than training a taxonomist. The above-mentioned potential usages combined with the fast processing capacity recommend PFCM for a more refined temporal and spatial monitoring, but also prompts its use for wide applications in experimental work. The increase in sampling frequency over time and space has already been used to gain more insight into phytoplankton dynamics (Dugenne et al. 2014, Thyssen et al. 2014, 2015, Bonato et al. 2015, 2016). Additionally, the present study demonstrates that carbon biomasses can be individually estimated by PFCM, based on live cells, allowing high-resolution biomass assessment. This high-resolution information contributes to our understanding of fine structures underlying phytoplankton distributions, ecology, and interactions. It is important to stress that with this kind of technology, the increase in data does not necessarily translate into increasing operational costs, even though initial costs for a PFCM apparatus are relatively high.

Drawbacks to the method are that clusters derived from PFCM have little taxonomic information, if not combined with other techniques like microscopy (light or electron), imaging-in-flow cytometry, or molecular tools. On the other hand, previous studies have shown that the PFCM can also operate as an imaging-in-flow cytometer for larger phytoplankton species (Dugenne et al. 2014, Thyssen et al. 2015). However, combining qualitative screening of live samples with quantitative measures from the PFCM, assigning species to well-defined clusters, is a relatively inexpensive alternative to existing phytoplankton-analysis methods. Taxonomic assignment to PFCM clusters can also be made based on the cell characteristics (e.g. size and shape, presence of phycobilins) and the individual optical profiles from PFCM, but this approach is time-consuming as well and therefore not suitable to perform on all samples analysed with the PFCM. Additionally, for some organisms (especially the ones forming coiling chains), volumes obtained from total FWS can be overestimated and would require special attention and different processing.

We believe that PFCM is suitable for analysing a whole phytoplankton community, including small picophytoplankton and larger chains/colonies (0.5 to 1000 µm), in contrast to other fast methods such as standard and image-in-flow cytometry (Dashkova et al. 2017). This is supported by tests where PFCM has been used to enumerate bacteria and recorded particles down to 0.2 µm (J. Jang pers. comm.). Results from the present study show that it can be used to quantify phytoplankton communities with different taxonomic composition, and outputs are comparable with the ones obtained with classical microscopy. However, it is important to highlight that the detection of small cells with weak signal intensity depends on instrument sensitivity. The range of detectable cell sizes is broadened for instruments having a dual pair of sensors, allowing both smaller and larger cells to be detected and enumerated precisely (Bonato et al. 2016). In contrast, instruments with only the low-sensitivity photomultiplier have a limited size-detection range and need specific tuning to detect smaller cells (Thyssen et al. 2014).

The empirical models and resulting formulas used in the present study to convert total FLR-hs and FWS to chl *a* and cell volume, respectively, enable PFCM results to be more comparable with traditional techniques. Importantly, information on live individual particles can also be used to assess differences in physiology (i.e. ratio of fluorescence per volume unit in the cells) and among populations (i.e. volume variability).

Acknowledgements. L.H. was supported by a grant from the Brazilian programme Science Without Borders/CAPES (grant no. 13581-13-9). H.H.J. received funding from the VELUX Foundation (grant no. VKR022608) to procure microscopes. The present work is a contribution from the BONUS COCOA project funded by the European Union's Seventh Framework Programme for Research (EU FP7) and the Danish Research Council.

LITERATURE CITED

Álvarez E, López-Urrutia Á, Nogueira E, Fraga S (2011) How to effectively sample the plankton size spectrum? A case study using FlowCAM. J Plankton Res 33: 1119–1133

Amann RI, Blinder BJ, Olson RJ, Chisholm SW, Devereux R, Stahl DA (1990) Combination of 16S rRNA-targeted oligonucleotide probes with flow cytometry for analyzing mixed microbial populations. Appl Environ Microbiol 56: 1919–1925

Bonato S, Christaki U, Lefebvre A, Lizon F, Thyssen M, Artigas LF (2015) High spatial variability of phytoplankton assessed by flow cytometry, in a dynamic productive coastal area, in spring: the eastern English Channel. Estuar Coast Shelf Sci 154:214–223

Bonato S, Breton E, Didry M, Lizon F and others (2016) Spatio-temporal patterns in phytoplankton assemblages in inshore-offshore gradients using flow cytometry: a case study in the eastern English Channel. J Mar Syst 156: 76–85

Boyer JN, Kelble CR, Ortner PB, Rudnick DT (2009) Phytoplankton bloom status: chlorophyll *a* biomass as an indicator of water quality condition in the southern estuaries of Florida, USA. Ecol Indic 9(Suppl):S56–S67

Camoying MG, Yñiguez AT (2016) FlowCAM optimization: attaining good quality images for higher taxonomic classification resolution of natural phytoplankton samples. Limnol Oceanogr Methods 14:305–314

Campbell D, Hurry V, Clarke AK, Gustafsson P, Oquist G (1998) Chlorophyll fluorescence analysis of cyanobacterial photosynthesis and acclimation. Microbiol Mol Biol Rev 62:667–683

Campbell L, Olson RJ, Sosik HM, Abraham A, Henrichs DW, Hyatt CJ, Buskey EJ (2010) First harmful *Dinophysis* (Dinophyceae, Dinophysiales) bloom in the U.S. is revealed by automated imaging flow cytometry. J Phycol 46:66–75

Campbell L, Henrichs DW, Olson RJ, Sosik HM (2013) Continuous automated imaging-in-flow cytometry for detection and early warning of *Karenia brevis* blooms in the Gulf of Mexico. Environ Sci Pollut Res Int 20:6896–6902

Choi JW, Stoecker DK (1989) Effects of fixation on cell volume of marine planktonic protozoa. Appl Environ Microbiol 55:1761–1765

Cullen JJ (1982) The deep chlorophyll maximim: comparing vertical profiles of chlorophyll *a*. Can J Fish Aquat Sci 39: 791–803

Culverhouse PF, Macleod N, Williams R, Benfield MC, Lopes RM, Picheral M (2014) An empirical assessment of the consistency of taxonomic identifications. Mar Biol Res 10:73–84

Dashkova V, Malashenkov D, Poulton N, Vorobjev I, Barteneva NS (2017) Imaging flow cytometry for phytoplankton analysis. Methods 112:188–200

Dubelaar GBJ, Geerders PJF, Jonker RR (2004) High frequency monitoring reveals phytoplankton dynamics. J Environ Monit 6:946–952

Dugenne M, Thyssen M, Nerini D, Mante C and others (2014) Consequence of a sudden wind event on the dynamics of a coastal phytoplankton community: an insight into specific population growth rates using a single cell high frequency approach. Front Microbiol 5:485

Dürselen CD, Burgmer T, Raabe T (2014) Development or improvement of standards in support of the Water Framework Directive - WP 7: guidance on the estimation of algal biovolume. European interlaboratory comparison for determination of phytoplankton biovolume 2014. Report CEN/TC 230-Mandate M/424, p 1–162

Edler L, Elbrächter M (2010) The Utermöhl method for quantitative phytoplankton analysis. In: Karlson B, Cusack C, Bresnan E (eds) Microscopic and molecular methods for quantitative phytoplankton analysis. IOC manuals and guides, no. 55. UNESCO, Paris, p 13–20

Falkowski PG, Barber RT, Smetacek V (1998) Biogeochemical controls and feedbacks on ocean primary production. Science 281:200–206

Gregor J, Maršálek B (2004) Freshwater phytoplankton quantification by chlorophyll *a*: a comparative study of in vitro, in vivo and in situ methods. Water Res 38:517–522

Harris GP (1980) Temporal and spatial scales in phytoplankton ecology. Mechanisms, methods, models, and management. Can J Fish Aquat Sci 37:877–900

Hasle G (1978) The inverted microscope method. In: Sournia A (ed) Phytoplankton manual—monographs on oceanographic methodology 6. UNESCO, Paris, p 88–96

Hillebrand H, Dürselen CD, Kirschtel D, Pollingher U, Zohary T (1999) Biovolume calculation for pelagic and benthic microalgae. J Phycol 35:403–424

Hinder SL, Hays GC, Brooks CJ, Davies AP, Edwards M, Walne AW, Gravenor MB (2011) Toxic marine microalgae and shellfish poisoning in the British Isles: history, review of epidemiology, and future implications. Environ Health 10:54

Hoagland P, Anderson DM, Kaoru Y, White AW (2002) The economic effects of harmful algal blooms in the United States: estimates, assessment issues, and information needs. Estuaries 25:819–837

Jakobsen HH (2012) Interkalibrering af fytoplanktonundersøgelser i marine områder 2012. Tek Rapp 17. DCE - Nationalt Center for Miljø og Energi, Aarhus Universitet, Roskilde (in Danish)

Jakobsen HH, Carstensen J (2011) FlowCAM: sizing cells and understanding the impact of size distributions on biovolume of planktonic community structure. Aquat Microb Ecol 65:75–87

Jakobsen HH, Markager S (2016) Carbon-to-chlorophyll ratio for phytoplankton in temperate coastal waters: seasonal patterns and relationship to nutrients. Limnol Oceanogr 61:1853–1868

Jakobsen HH, Carstensen J, Harrison PJ, Zingone A (2015) Estimating time series phytoplankton carbon biomass: inter-lab comparison of species identification and comparison of volume-to-carbon scaling ratios. Estuar Coast Shelf Sci 162:143–150

Kiefer DA (1973) Fluorescence properties of natural phytoplankton populations. Mar Biol 22:263–269

Lutz VA, Sathyendaranath S, Head EJH, Li WKW (2001) Changes in the in vivo absorption and fluorescence excitation spectra with growth irradiance in three species of phytoplankton. J Plankton Res 23:555–569

Lutz VA, Sathyendranath S, Head EJH, Li WKW (2003) Variability in pigment composition and optical characteristics of phytoplankton in the Labrador Sea and the Central North Atlantic. Mar Ecol Prog Ser 260:1–18

Marie D, Partensky F, Jacquet S, Vaulot D (1997) Enumeration and cell cycle analysis of natural populations of marine picoplankton by flow cytometry using the nucleic acid stain SYBR Green I. Appl Environ Microbiol 63: 186–193

Marshall HG, Lacouture RV, Buchanan C, Johnson JM (2006) Phytoplankton assemblages associated with water quality and salinity regions in Chesapeake Bay, USA. Estuar Coast Shelf Sci 69:10–18

McFarland MN, Rines J, Sullivan J, Donaghay P (2015) Impact of phytoplankton size and physiology on particulate optical properties determined with scanning flow cytometry. Mar Ecol Prog Ser 531:43–61

McGrady-Steed J, Harris PM, Morin PJ (1997) Biodiversity regulates ecosystem predictability. Nature 390:162–165

Menden-Deuer S, Lessard EJ (2000) Carbon to volume relationships for dinoflagellates, diatoms, and other protist plankton. Limnol Oceanogr 45:569–579

Montagnes DJS, Berges JA, Harrison PJ, Taylor FJR (1994) Estimating carbon, nitrogen, protein, and chlorophyll *a* from volume in marine phytoplankton. Limnol Oceanogr 39:1044–1060

Olson RJ, Sosik HM (2007) A submersible imaging-in-flow instrument to analyze nano- and microplankton: Imaging FlowCytobot. Limnol Oceanogr Methods 5:195–203

Pinto AMF, Von Sperling E, Moreira RM (2001) Chlorophyll-a determination via continuous measurement of plankton fluorescence: methodology development. Water Res 35:3977–3981

R Core Team (2015) R: a language and environment for statistical computing. R Foundation for Statistical Computing, Vienna. www.R-project.org

Reynolds CS (2006) The ecology of phytoplankton. Cambridge University Press, Cambridge

Rutten TPA, Sandee B, Hofman ART (2005) Phytoplankton monitoring by high performance flow cytometry: a successful approach? Cytometry A 64A:16–26

Salmaso N, Morabito G, Buzzi F, Garibaldi L, Simona M, Mosello R (2006) Phytoplankton as an indicator of the water quality of the deep lakes south of the Alps. Hydrobiologia 563:167–187

Shvalov AN, Surovtsev IV, Chernyshev AV, Soini JT, Maltsev VP (1999) Particle classification from light scattering with the scanning flow cytometer. Cytometry 37:215–220

Sieracki CK, Sieracki ME, Yentsch CS (1998) An imaging-in-flow system for automated analysis of marine microplankton. Mar Ecol Prog Ser 168:285–296

Soini JT, Chernyshev AV, Hänninen PE, Soini E, Maltsev VP (1998) A new design of the flow cuvette and optical set-up for the scanning flow cytometer. Cytometry 31: 78–84

Staehr PA, Testa J, Carstensen J (2017) Decadal changes in water quality and net productivity of a shallow Danish estuary following significant nutrient reductions. Estuar Coasts 40:63–79

Steele JH (1962) Environmental control of photosynthesis in the sea. Limnol Oceanogr 7:137–150

Stramski D, Mobley CD (1997) Effects of microbial particles on oceanic optics: a database of single-particle optical properties. Limnol Oceanogr 42:538–549

Strickland JDH, Parsons TR (1972) A practical handbook of seawater analysis. Fisheries Research Board of Canada, Ottawa

Sun J, Liu D (2003) Geometric models for calculating cell biovolume and surface area for phytoplankton. J Plankton Res 25:1331–1346

Takabayashi M (2006) The effect of nutrient availability and temperature on chain length of the diatom, *Skeletonema costatum*. J Plankton Res 28:831–840

Tarran GA, Heywood JL, Zubkov MV (2006) Latitudinal changes in the standing stocks of nano- and picoeukaryotic phytoplankton in the Atlantic Ocean. Deep-Sea Res II 53:1516–1529

Thyssen M, Mathieu D, Garcia N, Denis M (2008) Short-term variation of phytoplankton assemblages in Mediterranean coastal waters recorded with an automated submerged flow cytometer. J Plankton Res 30:1027–1040

Thyssen M, Grégori GJ, Grisoni JM, Pedrotti ML and others (2014) Onset of the spring bloom in the northwestern Mediterranean Sea: influence of environmental pulse events on the in situ hourly-scale dynamics of the phytoplankton community structure. Front Microbiol 5:387

Thyssen M, Alvain S, Lefèbvre A, Dessailly D and others (2015) High-resolution analysis of a North Sea phytoplankton community structure based on in situ flow cytometry observations and potential implication for remote sensing. Biogeosciences 12:4051–4066

Utermöhl H (1958) Zur Vervollkommnung der quantitativen Phytoplankton-Methodik. Schweizerbart, Stuttgart

Veldhuis MJW, Kraay GW (2000) Application of flow cytometry in marine phytoplankton research: current applications and future perspectives. Sci Total Environ 64: 121–134

Vives-Rego J, Lebaron P, Nebe-von Caron G (2000) Current and future applications of flow cytometry in aquatic microbiology. FEMS Microbiol Rev 24:429–448

Voss KJ, Balch WM, Kilpatrick KA (1998) Scattering and attenuation properties of *Emiliania huxleyi* cells and their detached coccoliths. Limnol Oceanogr 43:870–876

Winder M, Cloern JE (2010) The annual cycles of phytoplankton biomass. Philos Trans R Soc B 365:3215–3226

Zarauz L, Irigoien X (2008) Effects of Lugol's fixation on the size structure of natural nano-microplankton samples, analyzed by means of an automatic counting method. J Plankton Res 30:1297–1303

Zingone A, Harrison PJ, Kraberg A, Lehtinen S and others (2015) Increasing the quality, comparability and accessibility of phytoplankton species composition time-series data. Estuar Coast Shelf Sci 162:151–160

Editorial responsibility: Urania Christaki, Wimereux, France

Submitted: October 4, 2016; Accepted: June 7, 2017
Proofs received from author(s): August 9, 2017